Microstructural Characteristics of Ti-48Al-2Cr Alloy

J. Zhang, L. He, Y. Cui, and H. Ye

(Submitted 5 February 2001)

The microstructural characteristics of two-phase $\alpha_2 + \gamma$ titanium aluminide before and after deformation are investigated by transmission electron microscopy (TEM). The orientation relationships associated with the γ-γ combinations can be divided into three types: true twin, order domain, and pseudo-twin. Of the three orientation relationships, true twin accounts for more than 50%, which is most likely due to a minimization of interfacial energy related to misfit and interaction energy of interface atoms. During deformation, lamellar boundaries cause different resistance to the propagation of intersecting twin. Experimental observations and theoretical analysis consistently show that the resistance has the following sequence: $F_{120°} < F_{180°} < F_{60°} < F_{\alpha 2/\gamma}$.

Keywords deformation, transmission, electron microscopy, intermetallic, microstructure, TiAl, twin

1. Introduction

The lamellar structure of Ti_3Al + TiAl two-phase alloys has been studied since 1970.[1] In the past decade, particularly, there has been an enormous increase in the research development activity on TiAl-based compounds as potential lightweight high-temperature structural materials.[2–7] It is indeed well known that there exist a great many microstructures which result from numerous transformation modes occurring during various heat treatments and that the mechanical properties are strongly affected by the microstructure. Recently, Zghal *et al.* performed a quantitative transmission electron microscopy (TEM) analysis of the lamellar microstructure in TiAl-based alloys through conventional diffraction analysis in the dark-field mode.[8] The statistical result of the orientation relationships associated with the γ-γ combinations is attributed to a minimization of the elastic energy of the interfaces. This paper presents a thorough examination of the lamellar structure for the present alloy using microdiffraction analysis in order to come to a good understanding of the lamellar structure.

The plastic deformation of titanium aluminide alloys exhibits characteristics typical of deformation behavior of other intermetallic compounds. Twinning especially has often been observed to occur in multiple $1/6\langle 11\bar{2}\rangle\{111\}$ systems with nonparallel shear vectors, leading to extensive intersections among twin bands.[9–13] Twin intersections are important since they represent a potential locking mechanism that reduces the propagation of twinning dislocations. The knowledge of the resistance of lamellar boundaries to the intersecting twin is important in understanding the deformation behavior of the lamellar structure. Therefore, the deformation twin intersection was also examined in this paper to investigate the resistance of lamellar boundaries.

J. Zhang, L. He, Y. Cui, and **H. Ye,** Laboratory of Atomic Imaging of Solids, Institute of Metal Research, Chinese Academy of Sciences, Shenyang 110015, People's Republic of China. Contact e-mail: jxzhang@nrim.go.jp.

2. Experimental

2.1 Crystallography of Twin Related to γ-γ Laths

There are three possible orientation relationships between different γ variants, *i.e.*, 180° rotation twin (true twin), 120° rotational domain, and 60° rotation twin (pseudotwin). For the 180° rotation twin, the $[1\bar{1}0]$ direction of the twin domain is rotated by 180° with respect to the $[1\bar{1}0]$ direction of the matrix domain on the (111) plane and the stacking sequence of the (111) plane is reversed across the domain boundary. It is in the same case for the 120° or 60° rotation. Figure 1(a) to (d) describe the three orientation relationships in the (111) plane of the matrix or twin. The $[1\bar{1}0]$ direction of the matrix (Fig. 1a) is rotated by 180°, 120°, and 60° along the normal of the (111) plane, resulting in the three cases described in Fig. 1(b) to (d), respectively. Obviously, there exist the following three orientation relationships among different domains. (Note: any vector expressed in the coordinates associated with the parent matrix or the twin will be written with an M or a T subscript, respectively.)

For 180° rotation twin (true twin):

$$[\bar{1}10]_M // [1\bar{1}0]_T$$

$$[0\bar{1}1]_M // [01\bar{1}]_T$$

$$[10\bar{1}]_M // [\bar{1}01]_T$$

$$(111)_M // (111)_T$$

For 120° rotational domain:

$$[\bar{1}10]_M // [10\bar{1}]_T$$

$$[0\bar{1}1]_M // [\bar{1}10]_T$$

$$[10\bar{1}]_M // [0\bar{1}1]_T$$

$$(111)_M // (111)_T$$

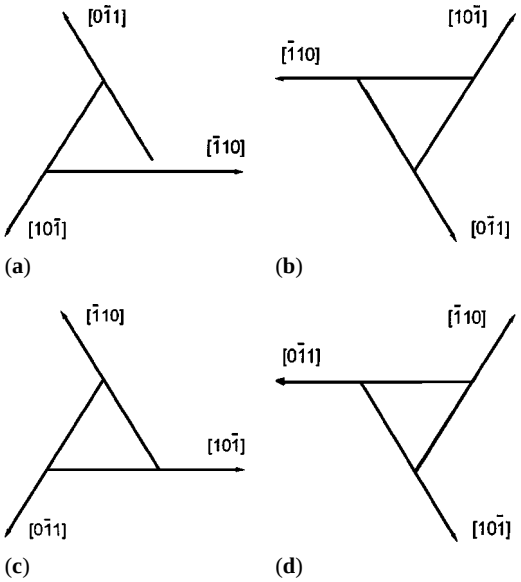

Fig. 1 Schematic representation of 180°, 120°, and 60° rotation twin relationships. The plane (111) is parallel to the paper plane. The [1$\bar{1}$0] direction of the matrix (**a**) is rotated by 180°, 120°, and 60° along the normal of the (111) plane resulting in the three cases (**b**) to (**d**) of the twin crystalline, respectively

For 60° rotation twin (pseudotwin):

$$[\bar{1}10]_M // [01\bar{1}]_T$$
$$[0\bar{1}1]_M // [\bar{1}01]_T$$
$$[10\bar{1}]_M // [1\bar{1}0]_T$$
$$(111)_M // (\bar{1}\bar{1}\bar{1})_T$$

The orientations of different lamellae were determined through conventional diffraction analysis. Experimental difficulties of this work arise from the fact that examinations sometimes have to be performed on very thin lamellae. In such a case, the habit plane has to be kept edge-on and the beam direction parallel with the ⟨110⟩ orientation of either twinned part. Meanwhile, the microdiffraction technique was used to differentiate the three twin relationships. Unfortunately, when the beam was located in the twin boundary zone, the resultant selected area electron diffraction (SAED) pattern was blurred and it was difficult to judge the types of possible twin relationships. There was no other selection but to obtain the SAED pattern of either plate of the twinned crystalline and then judge the possible twin relationships according to the method described in the following. The microdiffraction patterns of various orientations of single plate are shown in Fig. 2.

The experimental procedure to distinguish the three twin relationships is as follows:

- For the 120° rotational domains, the SAED patterns along the three zone axes described above are very interesting. There exists apparently only one set of SAED patterns from the matrix or twin because the {111}, {110}, and {100} planes in the matrix are parallel to those in the twin.

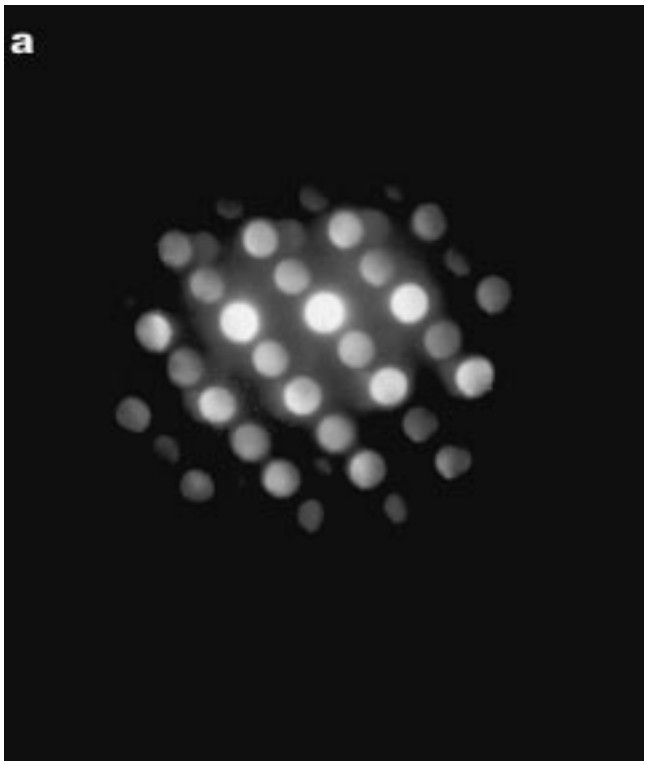

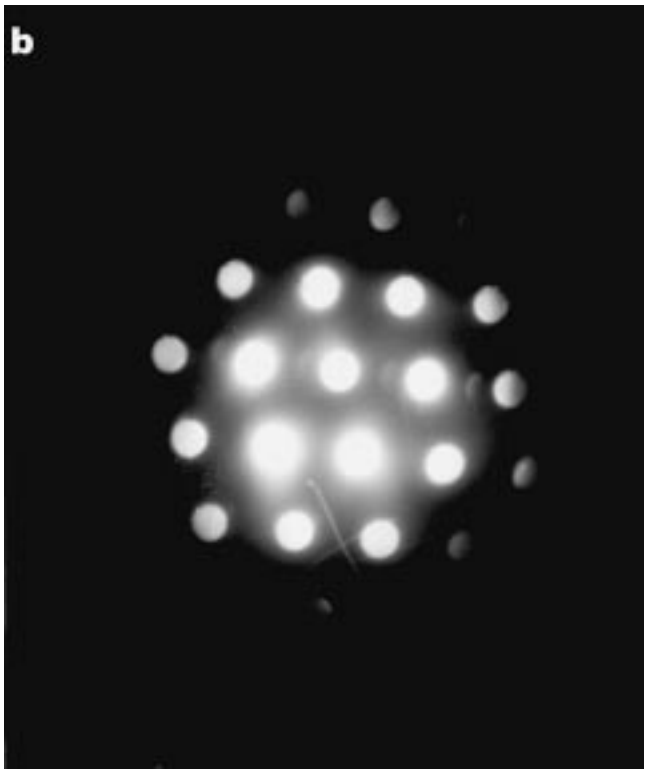

Fig. 2 Microdiffraction patterns: (**a**) [1$\bar{1}$0] or [$\bar{1}$10] and (**b**) [10$\bar{1}$], [$\bar{1}$01], [0$\bar{1}$1], or [01$\bar{1}$]

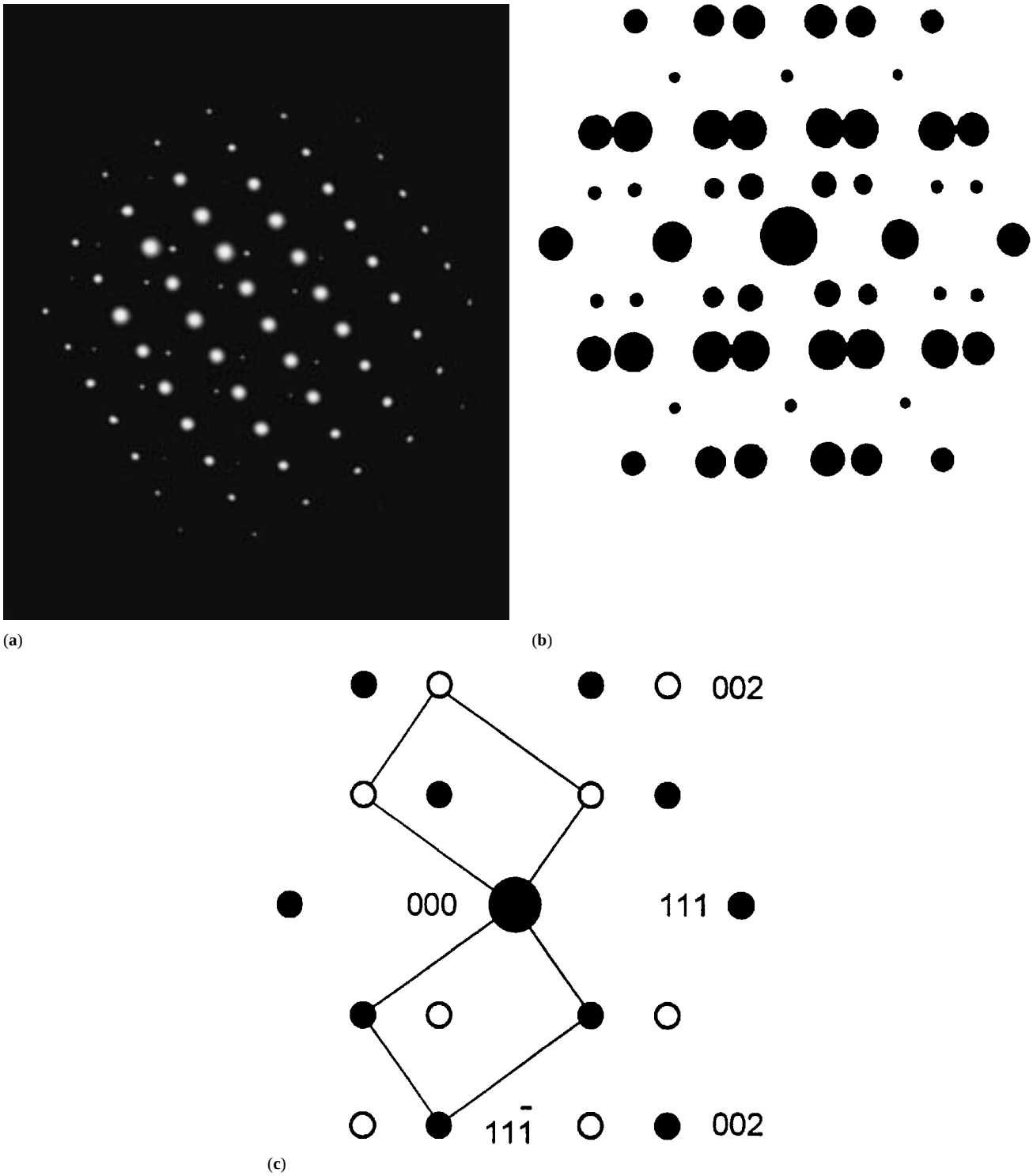

Fig. 3 (**a**) SAED pattern along the $[1\bar{1}0]_M//[\bar{1}10]_T$ orientation of true twin, (**b**) its schematic representation, and (**c**) indexed schematic diagram of the SAED pattern (solid circles stand for $[1\bar{1}0]$ zone and common spots, and open circles stand for $[\bar{1}10]$ zone spots)

- The SAED pattern of the $[1\bar{1}0]$ zone axis is distinguished from those along $[0\bar{1}1]$ or $[10\bar{1}]$ in its appearance of superlattice spots, as shown in Fig. 2(a), and (b). It is easy for us to find the $[\bar{1}10]_M//[1\bar{1}0]_T$ zone axis for true twin (Fig. 3) and the $[\bar{1}10]_M//[01\bar{1}]_T$ (or $[10\bar{1}]_M//[1\bar{1}0]_T$) for pseudotwin (Fig. 4), because there are two sets of superlattice spots and one set of superlattice spots, respectively.
- The SAED pattern of the $[0\bar{1}1]_M//[01\bar{1}]_T$ zone axis for true twin is similar with that of the $[0\bar{1}1]_M//[10\bar{1}]_T$ zone axis for pseudotwin (Fig. 5). After rotating by 60° along

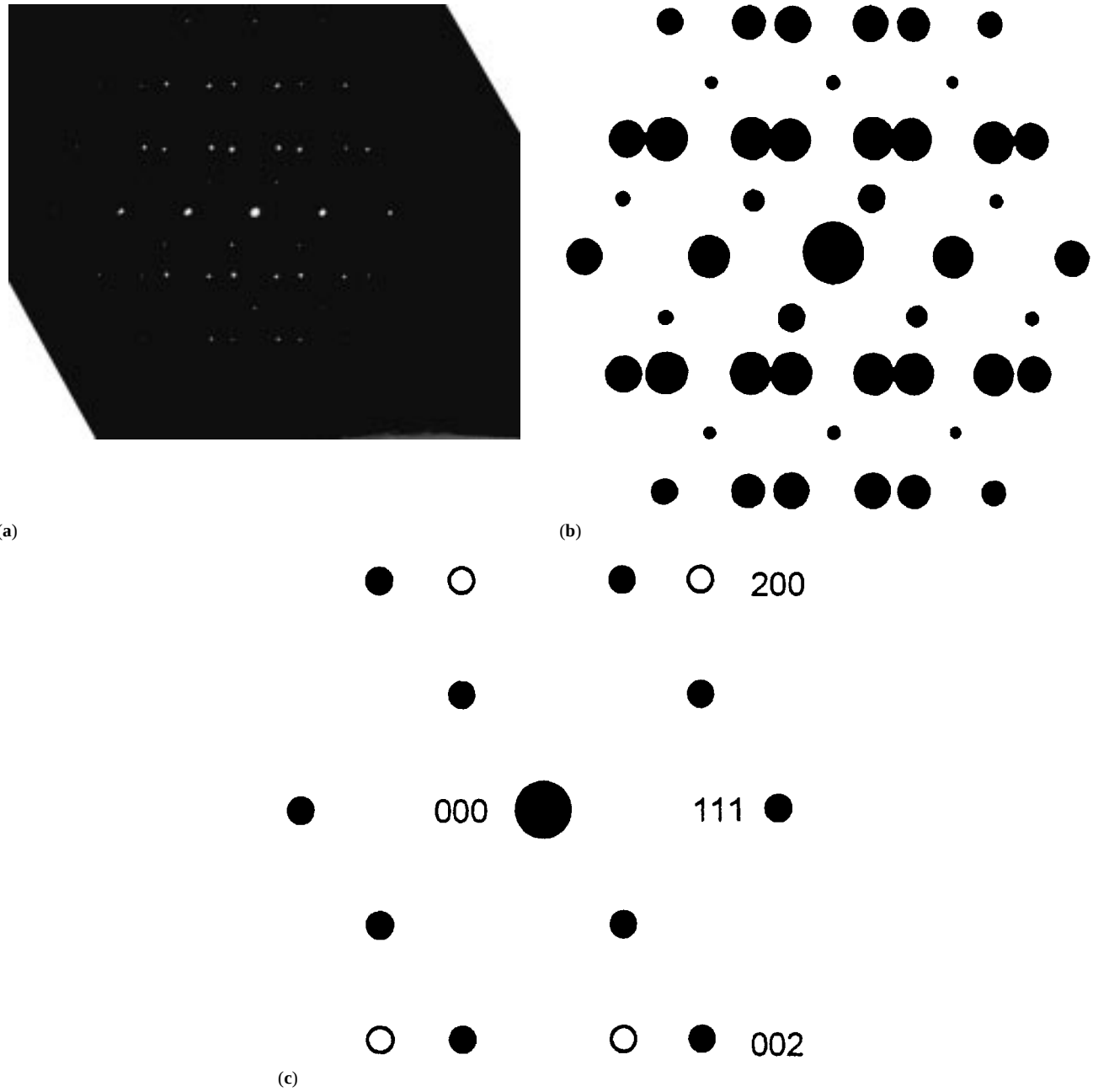

Fig. 4 (**a**) SAED pattern along the $[\bar{1}10]_M//[01\bar{1}]_T$ orientation of pseudotwin (similar case is the $[10\bar{1}]_M//[1\bar{1}0]_T$ orientation of pseudo-twin), (**b**) its schematic representation, and (**c**) indexed schematic diagram of the SAED pattern (solid circles stand for $[1\bar{1}0]$ zone and common spots, and open circles stand for $[01\bar{1}]$ zone spots)

the normal of the (111) plane, we can distinguish the two kinds of twins according to the resultant SAED pattern. If there exists only one set of superlattice spots, the twin orientation is of pseudotwin. Otherwise, if there exists two sets of superlattice ($[\bar{1}10]_M//[1\bar{1}0]_T$), or no superlattice spots ($[10\bar{1}]_M//[\bar{1}01]_T$), the twin orientation is of true twin.

2.2 Experimental Details

As-cast Ti-48Al-2Cr (at.%) alloy was produced by the skull-melting technique from high-purity materials. The ingot was encapsulated in quarts and heat treated as follows: each was homogenized for 10 h at 1100 °C, heated to 1225 °C, and held subsequently for 2 h before air cooling to room temperature. This heat treatment developed a lamellar microstructure. Compression coupons were cut from these heat-treated materials deformed at room temperature to 7% strain. Slices of both the heat-treated and deformed alloys were prepared for electron microscopy using standard techniques, and the thin foils were examined in a JEOL 2010 transmission electron microscope (Japan Electron Optics Ltd., Tokyo) operated at 200 kV.

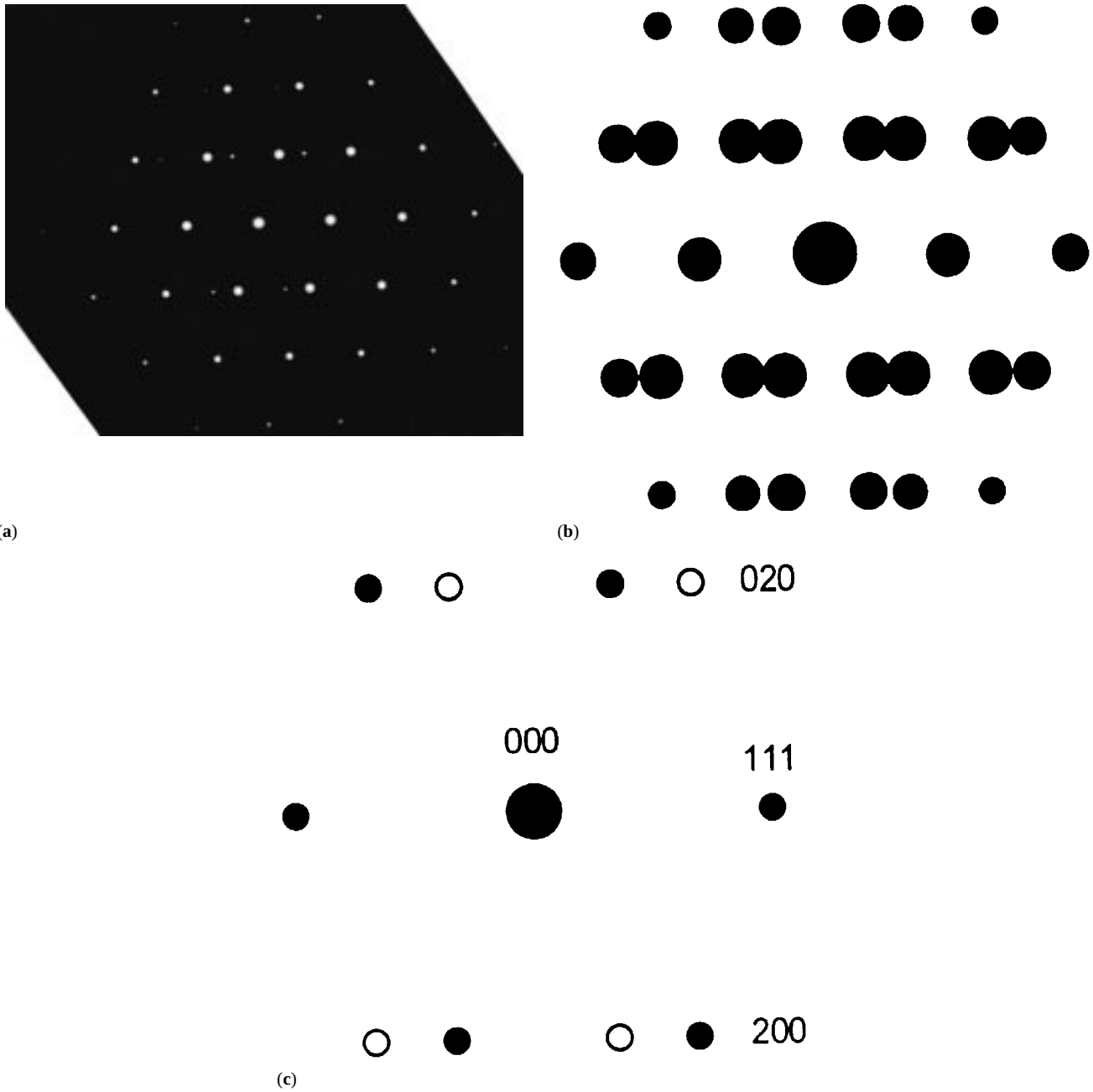

Fig. 5 (**a**) SAED pattern along the $[0\bar{1}1]_M//[\bar{1}01]_T$ orientation of pseudotwin (similar case is the $[0\bar{1}1]_M//[01\bar{1}]_T$ orientation or $[10\bar{1}]_M//[01\bar{1}]_T$ orientation of true twin), (**b**) its schematic representation, and (**c**) indexed schematic diagram of the SAED pattern (solid circles stand for $[0\bar{1}1]$ zone and common spots, and open circles stand for $[\bar{1}01]$ zone spots)

3. Results and Discussion

3.1 A Qualitative Description of Lamellar Structure

The TEM examination of specimens of the present alloy reveals a microstructure that exhibits alternating α_2 and γ lamellae (Fig. 6). The orientation relationships of α_2 and γ lamellae are $(0001)_{\alpha 2}//\{111\}_\gamma$ and $\langle 11\bar{2}0\rangle_{\alpha 2}//\langle 110\rangle_\gamma$. The lamellae are very thin. The widths of the primary α_2 and γ lamellae were 0.8 to 1.2 μm, and these lamellae were formed during $\alpha \rightarrow \alpha + \gamma \rightarrow \alpha_2 + \gamma$ transformations.[14]

The interfaces between γ and α_2 or γ and γ lamellae are very flat, lying parallel to each other. In the lamellar structure of two-phase TiAl compounds, there are four types of boundaries, as follows:

- γ/α_2 interphase boundaries;
- γ/γ domain boundaries, where the two neighboring domains are in true twin relation (180° rotation twin);
- γ/γ domain boundaries, where the two neighboring domains are in pseudotwin relation (60° rotation twin); and

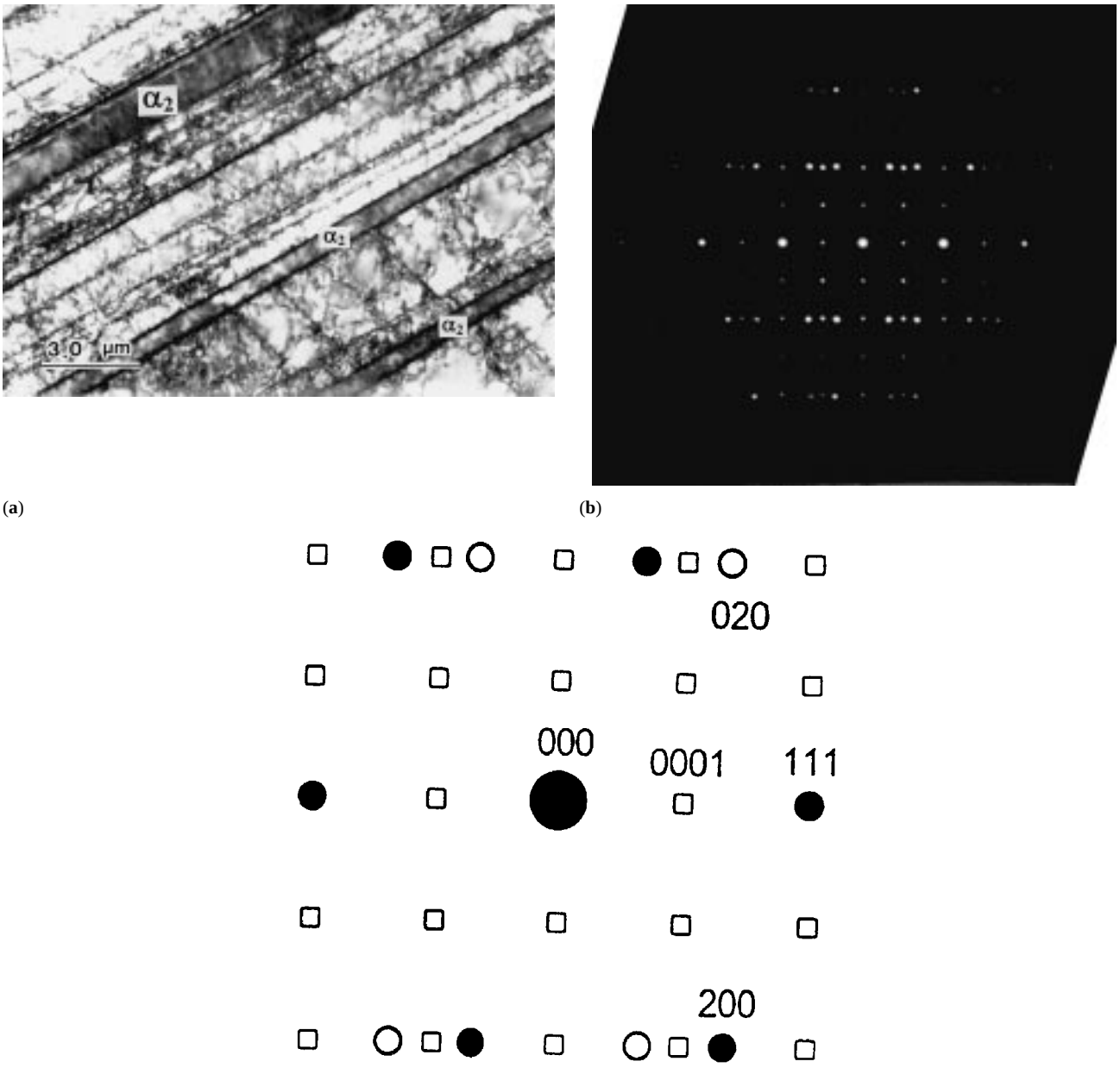

(**a**) (**b**)

(**c**)

Fig. 6 TEM micrograph of the Ti-48Al-2Cr alloy: (**a**) bright-field image of the twin-related γ laths and α_2 layers, (**b**) SAED pattern, and (**c**) indexed schematic diagram of the SAED pattern (solid circles stand for $[\bar{1}01]_\gamma$ zone and common spots, open circles stand for $[10\bar{1}]_\gamma$ zone spots, and rectangles stand for $[11\bar{2}0]_{\alpha 2}$ zone spots)

- 120° rotational γ/γ domain boundaries across which the stacking sequence of the (111) plane is maintained.

A quantitative analysis was made in different areas to count the percentage of the three kinds of γ-γ interface. The method for distinguishing is described in the experimental procedure. Thirty-six object spots are selected in different areas and different samples. Among the 36 γ-γ interfaces, 19 (representing 53%) belong to true twin boundaries, 6 (representing 17%) to 120° rotational domain boundaries, and 11 (representing 30%) to pseudotwin boundaries.

The occurrence of the true twin relationship is found to be more frequent than that corresponding to the pseudotwin or 120° rotational domain relationship. A higher fraction of the twin boundaries was also mentioned in Ref 15. This can be explained according to the misfit at the twin interfaces and the interaction energy of interface atoms, as described in the following sections.

Misfits in the Twinned γ-γ Interfaces. In the TiAl phase in equilibrium with the Ti_3Al phase, there are six different types of ordered domains corresponding to the six possible orientations for the $[1\bar{1}0]$ of TiAl with respect to the $\langle 11\bar{2}0\rangle$ of

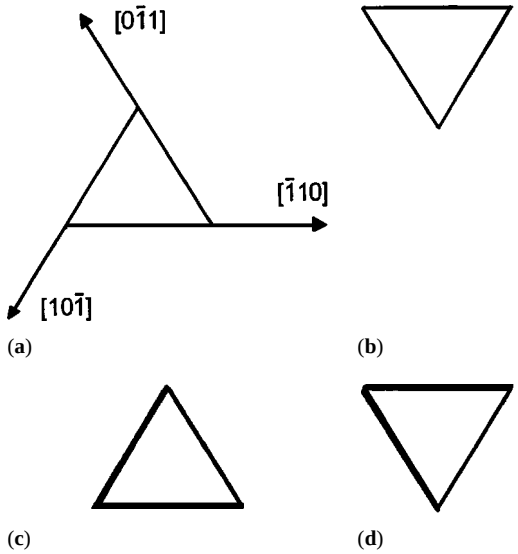

Fig. 7 Interfacial misfits associated with the tetragonality of the TiAl phase: (**a**) three ⟨110⟩ orientations in the (111) plane; (**b**) fully coherent true twin interface; (**c**) misfits along two directions $[\bar{1}10]_M//[10\bar{1}]_T$ and $[0\bar{1}1]_M//[\bar{1}10]_T$ in the 120° rotational domain interface; and (**d**) misfits along two directions $[\bar{1}10]_M//[01\bar{1}]_T$ and $[10\bar{1}]_M//[1\bar{1}0]_T$ in the pseudotwin interface

Ti_3Al. In the Ti_3Al phase, the three directions $[11\bar{2}0]$, $[1\bar{2}10]$, and $[\bar{2}110]$ are equivalent. However, due to the tetragonality in the TiAl phase, the $[1\bar{1}0]$ direction is not equivalent to the $\langle 10\bar{1}]$ or $\langle 01\bar{1}]$ direction. For the γ/γ_T domain combination, because the unit length in the $[10\bar{1}]$ direction is not equal to that in the $\langle 10\bar{1}]$ or $\langle 01\bar{1}]$ direction, misfitting exists along the $[1\bar{1}0]_\gamma//[10\bar{1}]_{\gamma T}$ or $[1\bar{1}0]_\gamma//[01\bar{1}]_{\gamma T}$, as shown in Fig. 7.

Because of the tetragonality of the $L1_0$ structure, the interfaces corresponding to the true twin relationship are fully coherent, while those corresponding to the pseudotwin relationship or 120° rotational domain relationship generate a mismatch. Kad and Hazzledine demonstrated that the misfit at {111} order interfaces might be accommodated, in principle, by either a cross-grid of edge dislocation, or a cross-grid of screw dislocation.[16] Therefore, the higher proportion found for the true twin relationship is most likely due to the minimization of the elastic energy of the interfaces. This minimization may be achieved through the following two processes.[8] One happens during the nucleation when collective or sympathetic ordering takes place involving several adjacent lamellae; in this case, adjacent variants are twin related to each other. The other process takes place during the growth when the migration of boundaries (pseudotwin boundaries or 120° rotational domain boundaries) separating two variants within each γ lamellar tends to reduce the pseudotwin portion or 120° rotational domain portion of the interface in favor of the twin relationship.

Interaction Energy of Interface Atoms. Interaction between interface atoms can contribute to the four kinds of interface. Inui *et al.* systemically compared the boundary energies of the three kinds of domain boundaries mentioned above by considering an AB compound with the $L1_0$ structure.[5] The energy γ_T of the true twin type lamellar boundary, the energy γ_P of the pseudo-twin-type lamellar boundary, and the energy γ_R of the 120° rotational domain boundary can be estimated roughly with a ratio of 1:7:6. This clearly explains why the true twin type lamellar domain boundaries are observed in the TiAl phase much more frequently than those of the 120° rotational and the pseudotwin types, consistent with the present observation.

3.2 TEM Observation of the Deformed Structure

Formation of Deformation Twins. After deformation, the most striking feature of the present alloy is the strong increase of the propensity of twinning. Figure 8 demonstrates the deformation structure deformed to 7% in pressure. Deformation twins (nearly vertical), having an angle of about 70° with the lamellar direction (nearly horizontal), consist of grid structure with lamellar plate. After a close examination of the lamellar plates, we find that there are several fine γ plates along the lamellar direction (shown by arrows). That is to say, deformation twins in the γ phase are also formed along the lamellar direction. In general, the width of these secondary γ laths was 0.1 to 0.2 μm.

Electron diffraction experiments for several different incident beam directions confirm that deformation twins corresponding to the fine structures are ordered (true) twins of the $(111)[11\bar{2}]$ type, which do not disturb the $L1_0$ symmetry of the lattice. In predominantly γ single-phase materials, {111} twins produced by 1/6⟨112] slip have been previously observed.[17] This observation was in agreement with another report,[18] which suggested that, because 1/6⟨121] and 1/6⟨211] slip will produce antiphase boundaries at the twin boundaries and are energetically disfavored, ⟨121]{111} and ⟨211]{111} twins will be forbidden and only ⟨112]{111} twins will be permitted in the $L1_0$ structure.

Besides the deformation twinning along the lamellar direction leading to the fineness of the lamellar structure, the transformation $\gamma \Leftrightarrow \alpha_2$ can also contribute to the plate fineness.[19,20] Because the atomic arrangements of stacking faults in α_2 are fcc, close to the γ structure, the γ phase may be easily produced from α_2 *via* formation of stacking faults during deformation. Similarly, because stacking faults in γ are hcp, α_2 may be produced from the γ phase during deformation.

Intersection of Deformation Twins: Some Observations. In most cases, shear deformation (mainly twinning) propagates across the lamellar boundaries almost in the one-to-one correspondence, but in some cases, the propagation is hindered by lamellar boundaries, as marked by S in Fig. 9. The lamellar boundaries in these cases are domain boundaries between differently oriented TiAl ordered domains. As seen in Fig. 9, some of the deformation twins impinge the lamellar boundaries and are stopped there. This indicates that, during deformation, the lamellar (domain) boundaries offer some resistance for the propagation of shear deformation. The deformation twin labeled T_1 originating from the 60° rotation twin boundary (position "O") penetrates through the 120° rotational domain boundary, but the propagation is hindered by another 60° rotation twin boundary (position "H"). Of interest is that the 120° boundary has little resistance to the propagation of deformation twin. Meanwhile, we also find that two deformation-induced γ plates (true twin) have no obvious resistance to the propagation of shear deformation.

Figure 10 is a high-magnification image of the lamellar

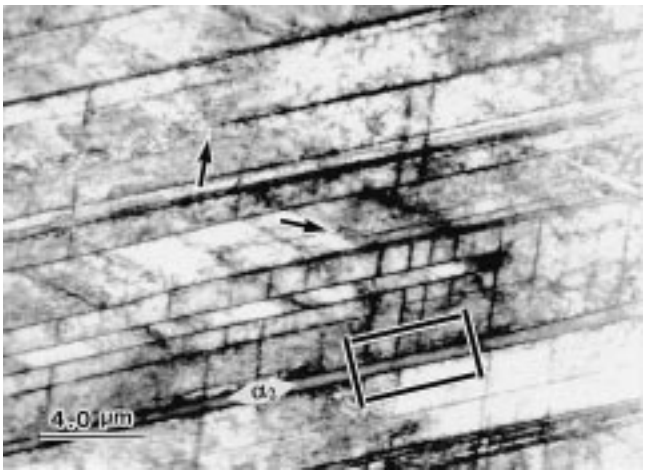

(**a**)

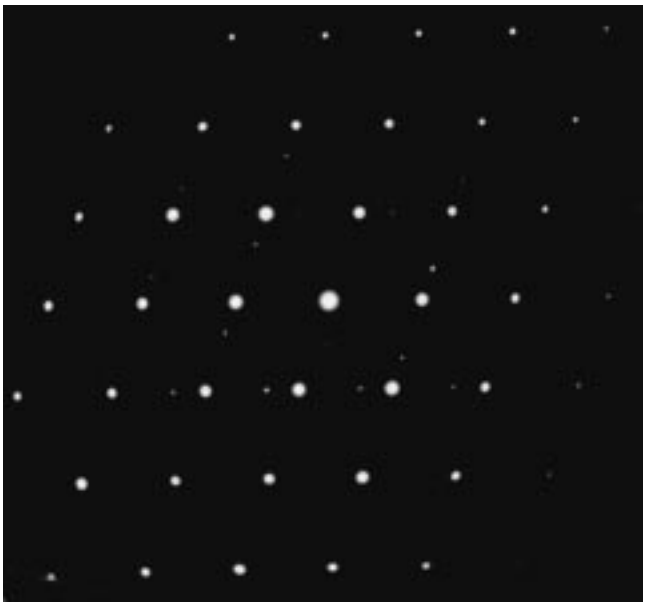

(**b**)

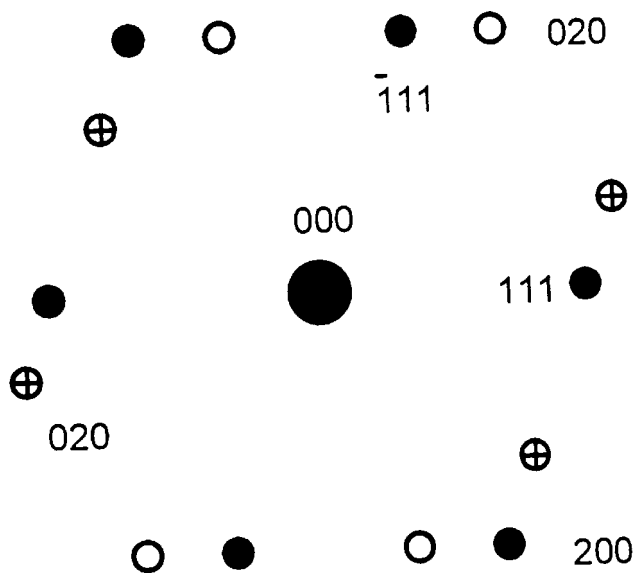

(**c**)

Fig. 8 TEM micrograph of the alloy deformed to 7%: (**a**) bright-field image of the twin-related γ laths, α_2 layers, and intersecting γ deformation twins; (**b**) SAED pattern; and (**c**) indexed schematic diagram of the SAED pattern (solid circles stand for $[0\bar{1}1]$ zone and common spots, open circles stand for $[10\bar{1}]$ zone spots, and cross-centered circles stand for $[\bar{1}01]_T$ zone spots)

structure, which shows another example of resistance of the lamellar boundaries for the propagation of shear deformation. In this case, 180° twin boundaries are marked in the figure. The deformation twin T_1, which originates from the α_2/γ interface, propagates along the direction shown by the arrow and is dragged at the 180° twin boundary. The distorted zone at the twin boundary shows that the boundary gives a considerable resistance to the propagation of deformation twin. After penetration through the 180° twin boundary, this deformation twin is hindered at another twin boundary, as marked by "S." In this micrograph, we cannot determine if the interface is 60° twin boundary. But, according to our many observations, the deformation twins are often terminated at 60° twin boundary.

A typical example showing the resistance by the lamellar boundaries for the propagation of shear deformation is shown in Fig. 11, which is an enlargement of the framed zone in Fig. 8. In this case, the lamellar boundaries are interphase boundaries between TiAl and Ti_3Al lamellae. Some deformation twins are seen to be stopped at the boundaries, indicating considerable resistance of the TiAl/Ti_3Al lamellar interphase boundaries for the propagation of deformation. A close examination of the Ti_3Al lamellar shown in Fig. 11 reveals a strain contrast, as

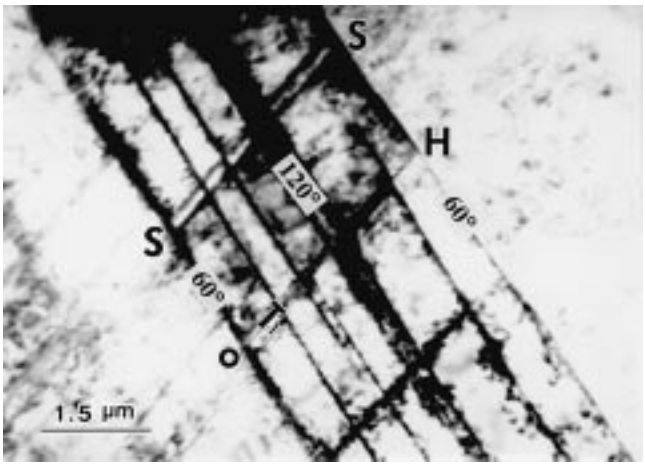

Fig. 9 TEM micrograph of the deformed alloy showing the twin intersection

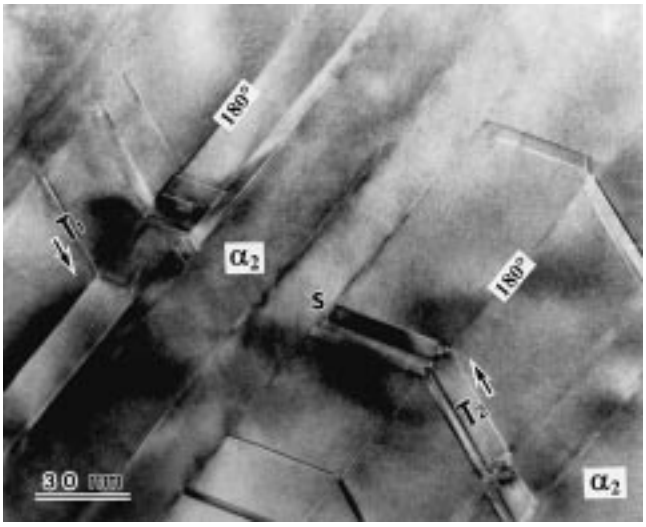

Fig. 10 High-magnification TEM micrograph showing the twin intersection

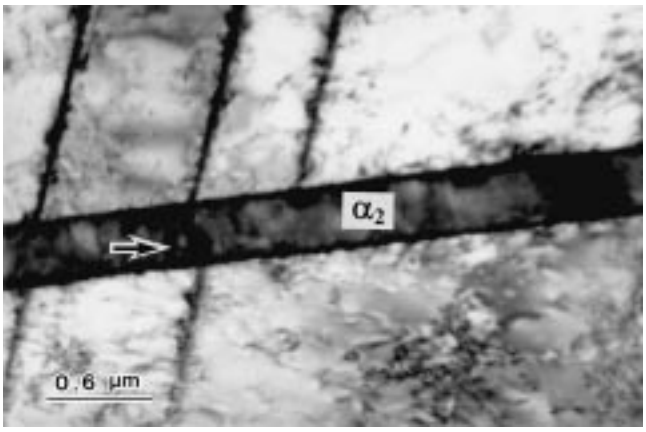

Fig. 11 High-magnification TEM micrograph of the framed area in Fig. 8

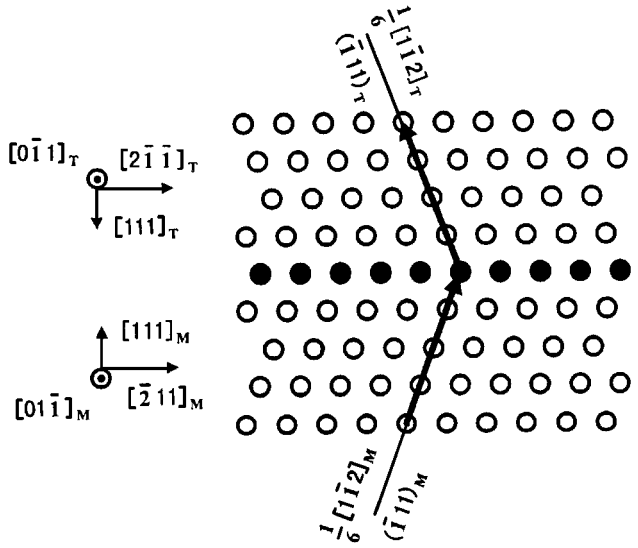

Fig. 12 Schematic diagram of the true twin structure viewed along $[0\bar{1}1]_M//[0\bar{1}1]_T$ (gray circle represents interface atom)

indicated by an arrow, but no glide dislocations are observed in the Ti_3Al lamellae. The Ti_3Al lamellae, in general, do not seem to be plastically deformed, at least at the stress level corresponding to the yielding of Ti-rich TiAl.

Intersection of Deformation Twins: Some Theoretical Considerations. Let us assume that a first mechanical twin (referred to as barrier twin or twin I) had habit plane (111) in the orientation relationship of 180° rotation twin (true twin), 120° rotational domain, or 60° rotation twin (pseudotwin). Any vector expressed in the coordinates associated with the parent matrix or the twin will be written with an M or a T subscript, respectively. A second twin (called incident twin or twin II) can hit the first on one of the $\{11\bar{1}\}$ plane by $1/6\langle 112\rangle$ partial dislocations. Now, we can examine the interaction between the $1/6\langle 112\rangle$ partial dislocation and the barrier twin or existing Ti_3Al plate.

- True twin

In this case, the true twin is the intersection line of the barrier twin and incident twin along the $[01\bar{1}]_M//[0\bar{1}1]_T$ direction. The incident twin (twin II) can shear the barrier twin on the $(\bar{1}11)_M$ plane by $\mathbf{b}_{i(M)} = 1/6[1\bar{1}2]_M$ partial dislocation, and thus, in the intersected twin coordinate system, they can expressed in the following vectors:

$$\frac{1}{3}\begin{pmatrix} 1 & -2 & -2 \\ -2 & 1 & -2 \\ -2 & -2 & 1 \end{pmatrix}\begin{pmatrix} -1 \\ 1 \\ 1 \end{pmatrix}_M = \frac{1}{3}(\bar{5}11)_T$$

and

$$\mathbf{b}_i = \frac{1}{3}\begin{pmatrix} 1 & -2 & -2 \\ -2 & 1 & -2 \\ -2 & -2 & 1 \end{pmatrix}\frac{1}{6}\begin{pmatrix} -1 \\ -1 \\ 2 \end{pmatrix}_M = \frac{1}{18}[\bar{1}\bar{7}2]_T$$

The only twin system for transmitting the incident twinning strain through twin I is $\mathbf{b}_b = 1/6[1\bar{1}2]_T(\bar{1}11)_T$, as shown in Fig. 12. The angle between the planes $(\bar{1}11)_M$ and $(\bar{1}11)_T$ can be

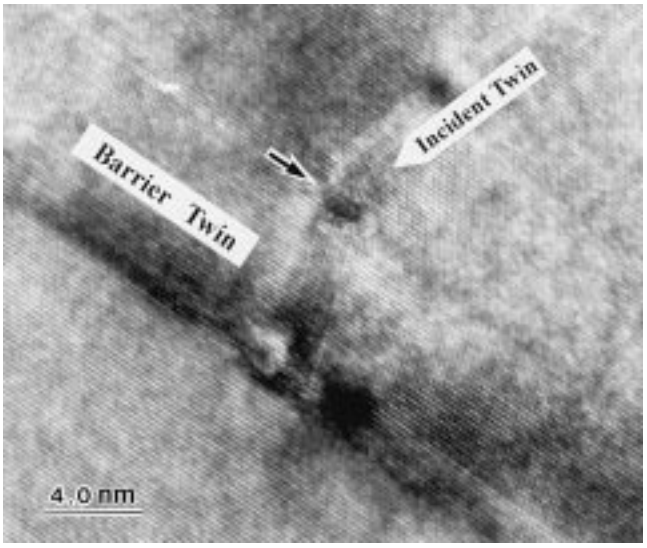

Fig. 13 Translation of twinning deformation across an interfacial boundary γ/γ_T between lamellae with true twin orientation. Foil orientation $\langle 01\bar{1}]$

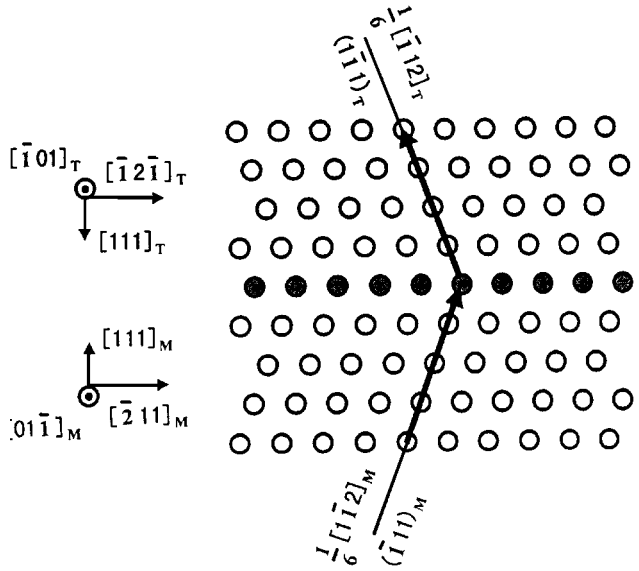

Fig. 14 Schematic diagram of the pseudotwin structure viewed along $[01\bar{1}]_M//[\bar{1}01]_T$ (gray circle represents interface atom)

computed to be 141°, consistent with the measured result in Fig. 10. Even though this angle is very large, such a situation still occurred according to the observation.

The difference **X** between the transmitted and the incident vector is

$$\mathbf{X} = \mathbf{b}_i - \mathbf{b}_b = \frac{1}{18}[\bar{1}\,\bar{7}2]_T - \frac{1}{18}[3\bar{3}6]_T = -\frac{2}{9}[111]_T$$

Thus, the intersecting twinning system leaves, at the matrix-twin I interface, a residual displacement given by the vector **X**. The magnitude of the **X** vector is fairly large (about 1.54 Å) when compared with the magnitude of the incident Burgers vectors (1.63 Å); thus, it would impose a strong backward stress on new incoming partials. In fact, we can notice the seriously distorted zone at the intersected matrix-twin I interface, as shown in Fig. 13, which results from the vector **X**.

- Pseudotwin

The orientation relationship of 60° pseudotwin is similar to that of 180° true twin. This determines that the interaction of the incident twin with the existing barrier twin is also similar to that of the 180° true twin, as analyzed above.

Suppose that the intersection line of the barrier twin and incident twin is along the $[01\bar{1}]_M//[\bar{1}01]_T$ direction. The habit plane of the incident twin is $(\bar{1}11)_M$, and the slip direction of the incident twin is $\mathbf{b}_{i(M)} = 1/6[1\bar{1}2]_M$. In the intersected twin coordinate system, the $\mathbf{b}_{i(M)}$ vector can be expressed as follows:

$$\mathbf{b}_i = \frac{1}{3}\begin{pmatrix} -2 & -2 & 1 \\ 1 & -2 & -2 \\ -2 & 1 & -2 \end{pmatrix}\frac{1}{6}\begin{pmatrix} 1 \\ -1 \\ 2 \end{pmatrix} = \frac{1}{18}[2\bar{1}\,\bar{7}]_T$$

If the strain were to be transferred as a transmitted twin, the slip direction would be $\mathbf{b}_b = 1/6[\bar{1}12]_T$ and the twin plane $(1\bar{1}\,\bar{1})_T$, as shown in Fig. 14. Therefore, the misfitting dislocation of Burgers vector **X** at the twin interface has a form similar to that in the 180° true twin:

$$\mathbf{X} = \mathbf{b}_i - \mathbf{b}_b = \frac{1}{8}[2\bar{1}\,\bar{7}]_T - \frac{1}{18}[\bar{3}36]_T = \frac{1}{18}[5\bar{4}\,\bar{1}\,\bar{3}]_T$$

Thus, similar to the true twin, the intersecting twinning system also leaves, at the matrix-twin I interface, a residual displacement given by the vector **X**. The magnitude of the **X** vector is fairly large (about 3.22 Å) when compared with the magnitude of the incident Burgers vectors (1.63 Å) and the residual displacement (1.54 Å) in the case of true twin.

- 120° rotational domain

Figure 15 is the orientation relationship of the 120° rotational domain. This orientation relationship is different from that of the 180° rotation twin (true twin) or 60° rotation twin (pseudotwin) discussed above. The {100}, {110}, and {111} planes of the matrix for this kind of twin are parallel to those of the twin.

Let us assume that the twin intersection occurs along the $[10\bar{1}]_M//[0\bar{1}1]_T$. The slip direction and slip plane of the incident twin are $\mathbf{b}_{i(M)} = 1/6[\bar{1}12]_M$ and $(1\bar{1}1)_M$, respectively, and thus, in the intersected twin coordinate system, they are expressed as follows:

$$\mathbf{b}_i = \begin{pmatrix} 0 & 1 & 0 \\ 0 & 0 & 1 \\ 1 & 0 & 0 \end{pmatrix}\frac{1}{6}\begin{pmatrix} -1 \\ 1 \\ 2 \end{pmatrix}_M = \frac{1}{6}[12\bar{1}]_T$$

and

$$\begin{pmatrix} 0 & 1 & 0 \\ 0 & 0 & 1 \\ 1 & 0 & 0 \end{pmatrix}\begin{pmatrix} 1 \\ -1 \\ 1 \end{pmatrix}_M = (\bar{1}11)_T$$

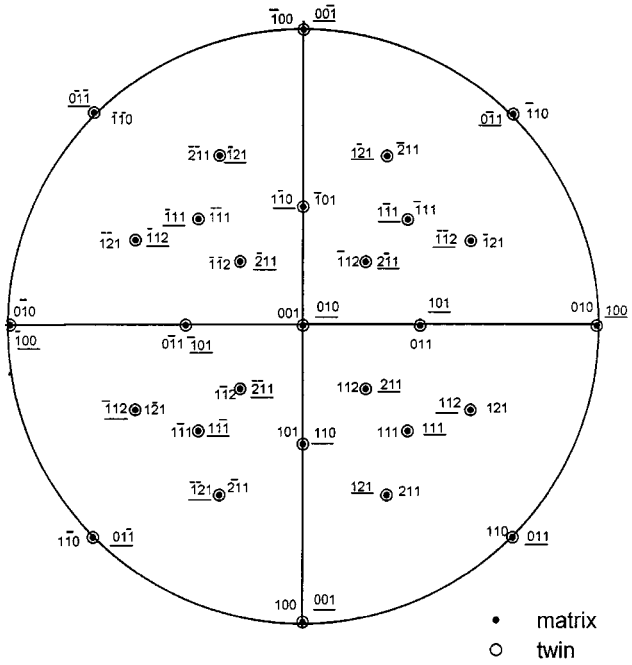

Fig. 15 Stereographic projection showing the orientation relationship of the 120° rotational domain

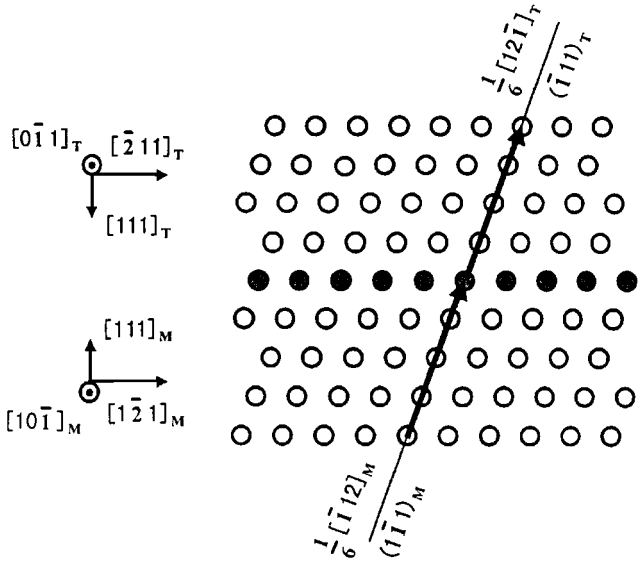

Fig. 16 Schematic diagram of the 120° rotational domain structure viewed along $[10\bar{1}]_M//[0\bar{1}1]_T$ (gray circle represents interface atom)

Due to the parallelism of $[\bar{1}12]_M//[12\bar{1}]_T$ and $(1\bar{1}1)_M//(\bar{1}11)_T$, the strain from the incident twin is easily transmitted through the barrier twin without a change of slip direction and slip plane, as shown in Fig. 16. Though as an alternative, it is reasonable to assume that the strain due to the incident twin is transferred as $\mathbf{b}_b = 1/6[1\bar{1}2]_T\ (\bar{1}11)_T$, this situation will also result in a residual displacement at the matrix-twin I interface:

$$\mathbf{X} = \mathbf{b}_i - \mathbf{b}_b = \frac{1}{6}[12\bar{1}]_T - \frac{1}{6}[1\bar{1}2]_T = \frac{1}{2}[01\bar{1}]_T$$

Comparatively, $1/6[12\bar{1}]_T$ slip without the residual displacement is energetically favored, though it will produce an antiphase boundary at the twin boundary.

- TiAl/Ti_3Al interphase interface

Yang[21] has shown $\langle 11\bar{2}0\rangle\{10\bar{1}0\}_{\alpha 2}$ to be the primary slip system in binary Ti-25Al. Activation of $\langle 11\bar{2}0\rangle(0001)_{\alpha 2}$ slip is difficult. The slip behavior of the Ti_3Al phase makes it difficult for the strain from the incident twin in the TiAl phase to be transmitted. Due to the orientation relationships $\{111\}_\gamma// \{0001\}_{\alpha 2}$ and $\langle 110\rangle_\gamma//\langle 11\bar{2}0\rangle_{\gamma 2}$, it is easy to calculate the angle between the $[112]_\gamma$ direction on the $\{11\bar{1}\}_\gamma$ plane, and the $\langle 11\bar{2}0\rangle_{\alpha 2}$ on the $(0001)_{\alpha 2}$ is more than 70.5° ($(11\bar{1}) \wedge (111) \approx 70.5°$). Therefore, it is unfavorable to activate slip dislocation in Ti_3Al. If the strain is large enough, the $\langle 11\bar{2}0\rangle(10\bar{1}0)$ may be activated. Because $\langle 11\bar{2}0\rangle_{\alpha 2}$ is parallel to the TiAl/Ti_3Al interface plane, we cannot see the penetration of the incident twin.

Therefore, all four types of boundaries in the lamellar structure may cause resistance to the propagation of deformation twins. According to the discussion, 120° rotational domain boundaries will cause the least resistance, since the direction of shear and the plane of shear will not be changed on the propagation of deformation. Regarding to the other three interfaces, the resistance F to the incident twin has the following sequence: $F_{180°} < F_{60°} < F_{\gamma/\alpha 2}$. Here, 180°, 60°, and γ/α_2 represent 180° rotation twin interface, 60° rotation twin interface, and γ/α_2 interphase interface, respectively.

4. Conclusions

- The relationships corresponding to γ-γ combinations can be true twin, 120° rotational domain, and pseudotwin. Among them, the twin relationship was most frequently observed. This is most likely due to a minimization of the interfacial energy associated with misfit and interaction energy of interface atoms.
- Plastic deformation leads to the appearance of twin intersection. The lamellar boundaries have different resistance to the propagation of intersecting twins. The 120° rotational domain boundary has the lowest resistance, and the other three cases have the following sequence: $F_{180°} < F_{60°} < F_{\alpha 2/\gamma}$.
- For the three orientation relationships related to the γ-γ combination, the resistance of lamellar interface to the intersecting twin is determined by the residual displacement between the transmitted vector and the incident vector.

References

1. M.J. Blackburn: in *The Science, Technology and Applications of Titanium*, R. Jaffee, and N.E. Promisel, eds., Pergamon Press, Oxford, United Kingdom, 1970, p. 406.
2. S.M.L. Sastry, and H.A. Lipsitt: in *Titanium '80*, H. Kimura, and O. Izumi, eds., TMS-AIME, Warrendale, PA, 1980, p. 1231.
3. M. Yamaguchi, S.R. Nishitani, and Y. Shirai: in *High Temperature Aluminides and Intermetallics*, S.H. Whang, C.T. Liu, D.P. Pope, and J.O. Stiegler, eds., TMS, Warrendale, PA, 1990, p. 63.

4. M. Yamaguchi, and Y. Umakoshi: *Progr. Mater. Sci.*, 1990, vol. 34, p. 1.
5. H. Inui, M.H. Oh, A. Nakamura, and M. Yamaguchi: *Phil. Mag. A*, 1992, vol. 66, pp. 539-55.
6. J. Luster, and M.A. Morris: *Metall. Mater. Trans. A*, 1995, vol. 26A, pp. 1745-56.
7. F. Appel, and R. Wagner: *Mater. Sci. Eng.*, 1998, vol. R22, pp. 187-268.
8. S. Zghal, S. Naka, and A. Couret: *Acta Mater.*, 1997, vol. 45, pp. 3005-15.
9. F. Appel, P.A. Beaven, and R. Wagner: *Acta Metall. Mater.*, 1993, vol. 41, pp. 1721-32.
10. S. Wardle, I. Phan, and G. Hug: *Phil. Mag. A*, 1993, vol. 67, pp. 497-514.
11. Y.Q. Sun, P.M. Hazzledine, and J.W. Christian: *Phil. Mag. A*, 1993, vol. 68, pp. 471-94.
12. Y.G. Zhang, and M. Chaturvedi: *Phil. Mag. A*, 1993, vol. 68, pp. 915-37.
13. M. Lonbradon, R. Bonnet, and J.M. Penisson: *Phil. Mag. A*, 1995, vol. 72, pp. 1381-95.
14. C. McCullough, J.J. Valencia, C.G. Levi, and R. Mehrabin: *Acta Metall.*, 1989, vol. 37, pp. 1321-36.
15. D. Dimiduk, Y.Q. Sun, and P. Hazzledine: *Mater. Res. Soc. Proc.*, 1995, vol. 364, p. 599.
16. B.K. Kad, and P.M. Hazzledine: *Phil. Mag. Lett.*, 1992, vol. 66, pp. 133-39.
17. D. Shechtman, M.J. Blackburn, and H.A. Lipsitt: *Metall. Trans.*, 1974, vol. 5, pp. 1373-81.
18. D.W. Pashley, J.L. Robertson, and M.J. Stowell: *Phil. Mag.*, 1969, vol. 19, p. 83.
19. Y. Gao, J. Zhu, H.M. Shen, and Y.N. Wang: *Scripta Metall.*, 1993, vol. 28, pp. 651-56.
20. Y.G. Zhang, F.D. Tichelaar, F.W. Schapink, Q. Xu, and C.Q. Chen: *Scripta Metall.*, 1995, vol. 32, pp. 981-85.
21. W.J.S. Yang: *Metall. Trans. A*, 1982, vol. 13A, pp. 324-28.